

Near-Field Photometric Stereo in Ambient Light

Fotios Logothetis¹

fl302@cam.ac.uk

Roberto Mecca^{1,2}

roberto.mecca@eng.cam.ac.uk

Yvain Quéau³

yvain.queau@enseeiht.fr

Roberto Cipolla¹

cipolla@eng.cam.ac.uk

¹ Department of Engineering

University of Cambridge

United Kingdom

² Department of Mathematics

University of Bologna

Italy

³ Université de Toulouse

France

Contents

1	Second Order Approximation	1
2	Additional Synthetic Dataset	2
3	Additional Real Dataset	5

1 Second Order Approximation

In this section we elaborate on how more than four images can be used to cancel up to the second order remainder of the Binomial expansion, that was briefly mentioned at the end of Section 3.

Starting from the same irradiance equation:

$$I_i(x, y) = \rho(x, y) a_i(x, y) (\bar{\mathbf{n}} \cdot \bar{\mathbf{h}}_i)^{\frac{1}{c}} + A(x, y) \quad (1)$$

our aim is now to show how to obtain a second order truncation of the following Binomial expansion:

$$(I_i - A)^c = (\rho a_i)^c \bar{\mathbf{n}} \cdot \bar{\mathbf{h}}_i \quad (2)$$

while considering triple of images. Let us start by taking into account the expansion till the third order:

$$I_i^c - c A I_i^{c-1} + \frac{c(c-1)}{2} A^2 I_i^{c-2} + \frac{c(c-1)(c-2)}{6} A^3 I_i^{c-3} + \dots = (\rho a_i)^c \bar{\mathbf{n}} \cdot \bar{\mathbf{h}}_i \quad (3)$$

and combining the previous equation for images i^{th} and j^{th} as follows:

$$\frac{(3)_i}{I_i^{c-1}} - \frac{(3)_j}{I_j^{c-1}} \quad (4)$$

we obtain:

$$I_i^c + \frac{c(c-1)}{2} A^2 I_i^{-1} - I_j^c - \frac{c(c-1)}{2} A^2 I_j^{-1} \approx \rho^c \gamma_i \bar{\mathbf{n}} \cdot \bar{\mathbf{h}}_i - \rho^c \gamma_j \bar{\mathbf{n}} \cdot \bar{\mathbf{h}}_j \quad (5)$$

where $\gamma_i = \frac{a_i^c}{I_i^{c-1}}$ and equivalently for the other indexes. The previous approximation yields the following:

$$\alpha_{ij}(I_i - I_j) + A^2 \approx \alpha_{ij}(\rho^c \gamma_i \bar{\mathbf{n}} \cdot \bar{\mathbf{h}}_i - \rho^c \gamma_j \bar{\mathbf{n}} \cdot \bar{\mathbf{h}}_j). \quad (6)$$

In order to consider ratio of those quantities, we derive the following equation considering the images i^{th} , j^{th} , k^{th} and p^{th} , q^{th} , r^{th} as:

$$\frac{(6)_{ij} - (6)_{ik}}{(6)_{pq} - (6)_{pr}} \quad (7)$$

that is

$$\frac{\alpha_{ij}(I_i - I_j) - \alpha_{ik}(I_i - I_k)}{\alpha_{pq}(I_p - I_q) - \alpha_{pr}(I_p - I_r)} \approx \frac{\alpha_{ij}(\gamma_i \bar{\mathbf{n}} \cdot \bar{\mathbf{h}}_i - \gamma_j \bar{\mathbf{n}} \cdot \bar{\mathbf{h}}_j) - \alpha_{ik}(\gamma_i \bar{\mathbf{n}} \cdot \bar{\mathbf{h}}_i - \gamma_k \bar{\mathbf{n}} \cdot \bar{\mathbf{h}}_k)}{\alpha_{pq}(\gamma_p \bar{\mathbf{n}} \cdot \bar{\mathbf{h}}_p - \gamma_q \bar{\mathbf{n}} \cdot \bar{\mathbf{h}}_q) - \alpha_{pr}(\gamma_p \bar{\mathbf{n}} \cdot \bar{\mathbf{h}}_p - \gamma_r \bar{\mathbf{n}} \cdot \bar{\mathbf{h}}_r)} \quad (8)$$

where $\alpha_{ij} = \frac{1}{I_i^{-1} - I_j^{-1}}$, and equivalently for the other indexes.

Expanding Equation 8, gives a linear relation for the normal \mathbf{n} which in turn can be expressed as a variational problem for the depth z shown in the main paper.

Note that the method presented above is much more complicated than the first order approximation that we used in the paper and so we left this for a future work.

2 Additional Synthetic Dataset

In this section, we present an additional synthetic dataset (using the "Armaddillo" model from The Stanford 3D Scanning Repository <http://graphics.stanford.edu/data/3Dscanrep/>). Again, the comparison is with Yuille *et al.* [14], Ikehata *et al.* [15] and Mecca and Quéau [16] on the case of orthographic viewing and Lambertian reflectance.

The Armaddillo dataset confirms the findings of section 5.1: our method achieves marginally better results than [14] and clearly outclasses [15, 16] as these two methods do not take the ambient light into account.

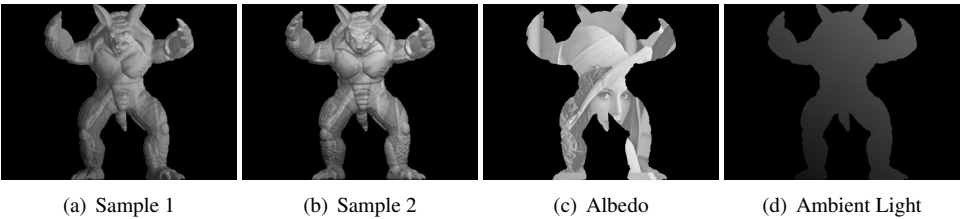


Figure 1: 1(a),1(b) are 2 out of the 24 images of our second simplified synthetic dataset rendered with orthographic geometry, directional lighting and Lambertian reflection. 1(c) shows the non-uniform albedo used. 1(d) shows the non-uniform ambient used.

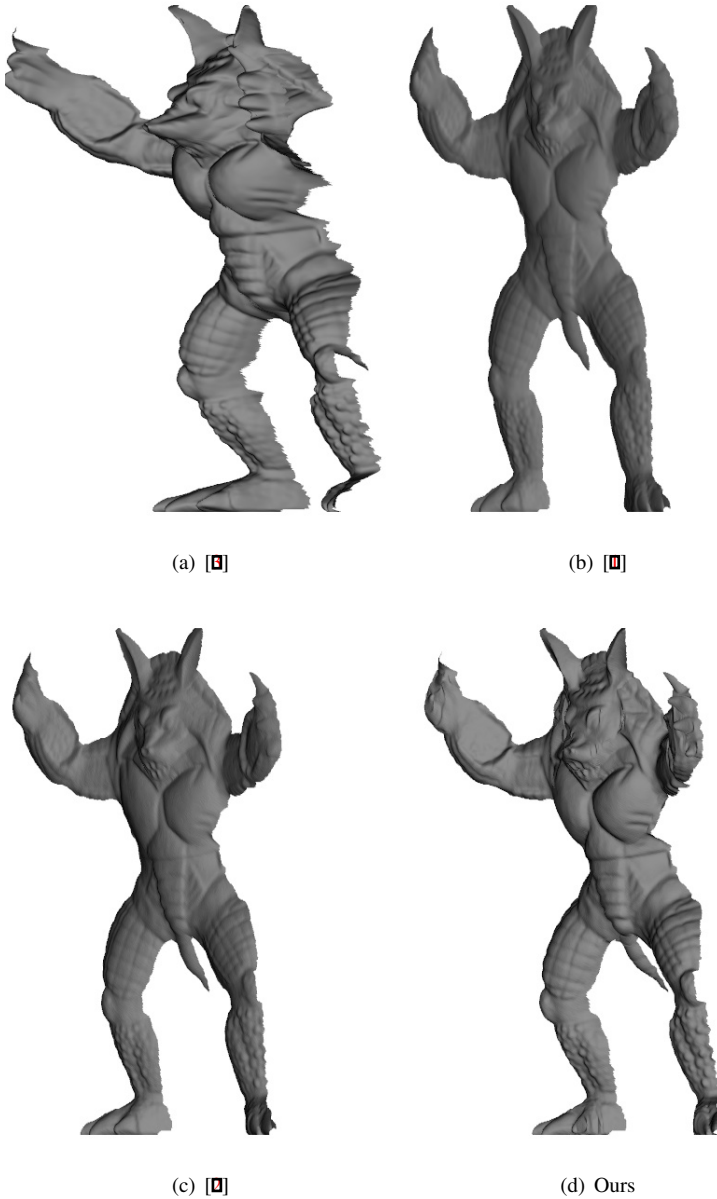


Figure 2: Comparison of several PS methods on the dataset of Figure 1. Note that 2(b) and 2(c) have a substantial flattening due to the ambient light.

Figure 4 shows how the mean normal error varies with different levels of mean ambient light. For all four methods, we performed 15 experiments; we consider 3 different levels of shininess ($c = 1$ i.e. Lambertian, $c = 0.7$ i.e. slight specular and $c = 0.4$ moderate specular) and 5 levels of mean ambient (from around 0.1 to 0.7 with 1 being the maximum intensity value). The virtual light source intensity was kept constant throughout the whole se-

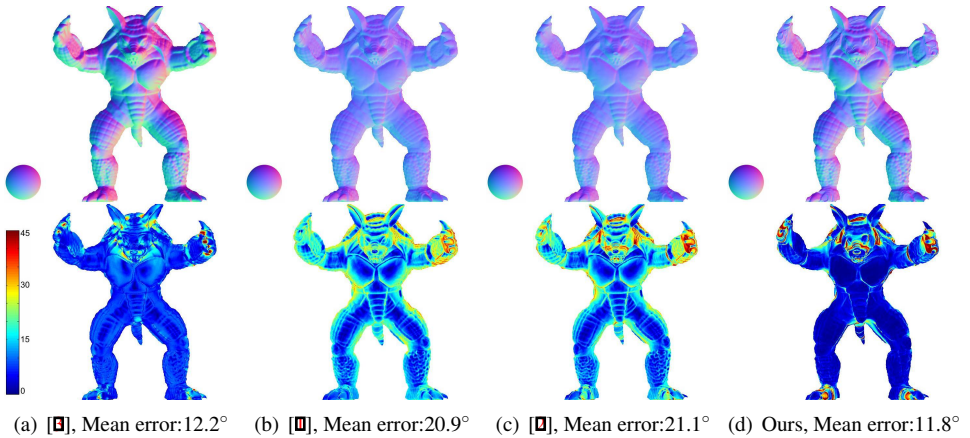


Figure 3: Quantitative evaluation of several PS methods on the dataset of Figure 1. Most errors are observed around the occlusion boundaries as expected.

quence to 0.3 (that is the value that pixels would get if there was no ambient, the albedo was 1 and the normal was aligned to the light direction). The important result of this experiment is that for methods not considering the ambient light ([1], [2]), the error increases steadily as the ambient light is increased. In contrary, [3] takes the ambient light into account so the error is independent of the mean ambient value (of course, as the ambient light approaches the maximum image intensity, a significant portion of the pixels become saturated and hence the performance of all methods degrades). Finally, for our method, the error is independent of the ambient when $c = 1$ and it is very slightly increasing as the ambient increases when $c \neq 1$; this is a direct consequence of the approximation of the Binomial series used by our method.

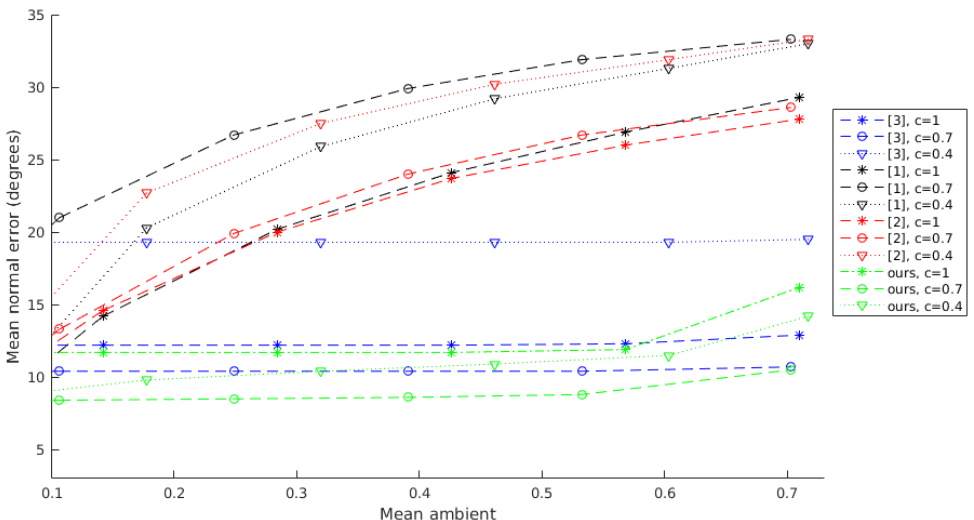


Figure 4: Comparison of several PS methods under different ambient light and shininess parameter. At high ambient levels, the error is dominated by the saturated pixels.

3 Additional Real Dataset

In this section, we present an additional real dataset. This includes 24 images of a shiny, wooden elephant miniature taken under significant artificial ambient light (Figure 5). This is quite a challenging dataset as it includes significant ambient light, some depth discontinuities around the legs as well as a moderate amount of specularities. Once again, we outclass all of our competing methods.

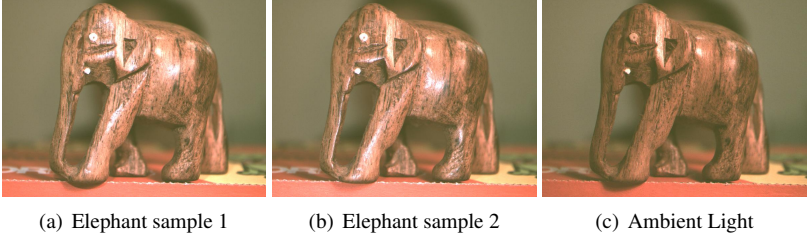


Figure 5: 2 sample images from the elephant dataset and the respective ambient light.

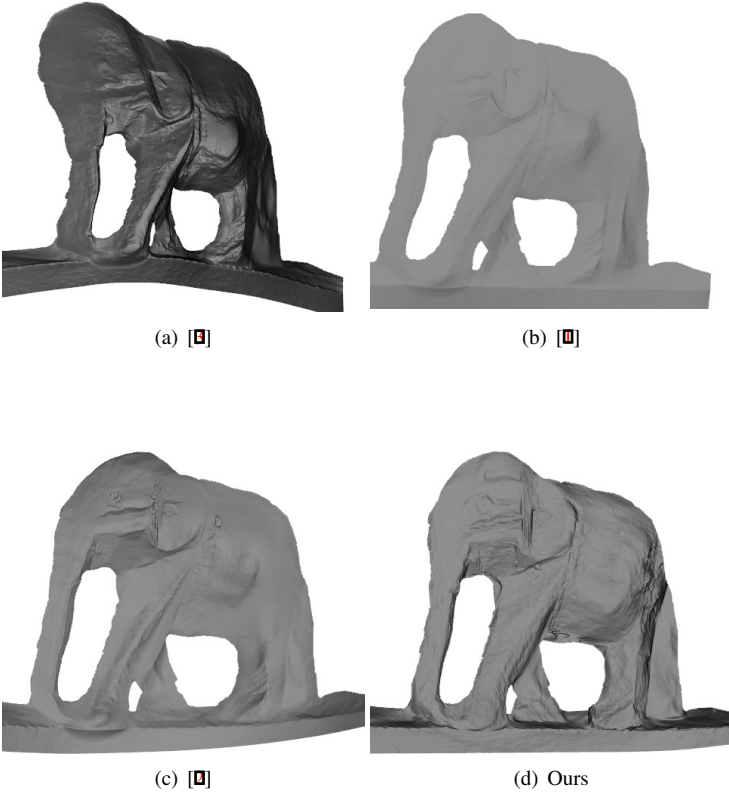


Figure 6: Comparison of several PS methods on the elephant dataset of Figure 5.

References

- [1] S. Ikehata, D. Wipf, Y. Matsushita, and K. Aizawa. Robust photometric stereo using sparse regression. In *CVPR*, 2012.
- [2] R. Mecca and Y. Quéau. Unifying diffuse and specular reflections for the photometric stereo problem. In *WACV*, 2016.
- [3] A. L. Yuille, D. Snow, R. Epstein, and P. N. Belhumeur. Determining generative models of objects under varying illumination: Shape and albedo from multiple images using SVD and integrability. *IJCV*, 35(3):203–222, 1999.